MODIFICATION OF PLANCK BLACKBODY RADIATION BY PHOTONIC BAND-GAP STRUCTURES

Christopher M. Cornelius and Jonathan P. Dowling*

Scientific and Technical Office (Optical Sciences)
Weapons Sciences Directorate, AMSAM-RD-WS-ST, Bldg. 7804
Missile Research, Development, and Engineering Center
U. S. Army Aviation and Missile Command
Redstone Arsenal, Alabama 35898-5000

(Received:)

ABSTRACT

We discuss a simple 1D model of the modification of Planck blackbody radiation by photonic band-gap materials (PBGs). The model gives qualitative predictions for the thermal power spectrum of 2D and 3D PBG structures, and quantitative results for 1D, distributed Bragg reflecting PBG thin films.

PACS: 42.50.Ct, 42.70.Qs, 78.20,Ci, 78.66.–w

I. INTRODUCTION

One of the most interesting subfields of quantum optics is cavity QED — where microcavities impose nontrivial boundary conditions on the quantized electromagnetic field and alter the matter-light interactions of quantum electrodynamics. One of the first predictions of this theory was the modification of atomic spontaneous emission rates, through the use of microcavities to alter the optical density of modes from its free-space value. This phenomenon is often known as the Purcell effect [1]. Since this prediction, many theoretical analyses [2] as well as experimental confirmations [3] of this effect have been performed. Since the imposition of nontrivial boundary conditions modifies the electromagnetic Green's function, the Feynman diagrams for *any* QED process must be altered in a cavity, giving physical results that differ from those in free space.

Version 4.0, 20 Nov 98
submitted to Phys. Rev. A

Some examples of these cavity QED effects are: cavity-induced changes in the Lamb shift [4], and the electron's gyromagnetic ratio (g–2) [5], Rutherford scattering near mirrors [6], and Raman scattering between mirrors [7].

Initially, most of these developments were discussed in the context of simple geometric structures, such as parallel-plane conducting cavities or 1D Fabry-Perot resonators composed from two distributed Bragg-reflecting mirrors. However, in the late 1980s and early 1990s the existence was demonstrated, both theoretically and experimentally of 2D and 3D periodic dielectric and metallo-dielectric structures that exhibit full, omni-directional photonic stop bands (or band gaps) for both degrees of photon polarization [8,9]. Initially, the primary interest in these materials was to alter atomic spontaneous emission rates — for instance to suppress them in order to produce a thresholdless microlaser [8,9]. Several theoretical and experimental [10–19] studies of the emission process in PBGs have appeared, but usually the emitters are considered to be pumped electrically or optically — not thermally.

In section II, we will review some of the theory related to the calculation of thermal power spectrum. In section III, we will discuss how a finite 2D or 3D PBG structure can be qualitatively studied using a 1D formalism, following a model originally developed by John and Wang [10]. In the context of this model, we compute the thermal power spectrum of a PBG filter in front of an emitting hot surface, as well as that of a heated PBG structure. In section IV, we produce a quantitative theory for studying the off-axis spectrum of 1D PBG structures of the DBR type. Finally, in section V we summarize and conclude.

II. BLACKBODY RADIATION, EMITTANCE, AND NORMAL MODES

A. Blackbody Radiation

Thermal radiation is just spontaneous emission that is thermally pumped and that has a blackbody spectrum, which is in thermal equilibrium with its

surroundings. From the foundations of quantum mechanics, it is well known that atomic oscillators in thermal equilibrium with a photon heat bath at temperature T have an average energy ε at frequency ω given by the Planck expression [20]

$$\varepsilon(\omega,\beta) = \frac{\hbar\omega}{e^{\hbar\omega\beta}-1}, \tag{1}$$

where

$$\beta \equiv \frac{1}{k_B T}, \tag{2}$$

as usual, with k_B the Boltzmann constant. The energy density per unit frequency $\mathcal{U}$ can be written as

$$\mathcal{U}(\omega,\beta) = \rho(\omega)\ \varepsilon(\omega,\beta), \tag{3}$$

where $\rho(\omega)$ is the electromagnetic density of modes. Crucial to our discussion here is that the modification of the density of modes ρ, by introduction of a cavity or PBG structure, say, will alter the energy density and hence the radiant power, $\mathcal{P}$, given by [20]

$$\mathcal{P}(\omega,\beta) = \frac{1}{4} c\, \mathcal{U}(\omega,\beta), \tag{4}$$

where c is the vacuum speed of light. $\mathcal{P}(\omega)$ is the radiant power per unit area emitted by the surface of a perfect blackbody. For free-space boundary conditions, the density of modes ρ^{FS} has the well-known form

$$\rho^{FS}(\omega) = \frac{2\omega^2}{\pi c^3}, \tag{5}$$

from which the blackbody power $\mathcal{P}^{BB}$ takes its usual form of the *Planck Law* [19]

$$\mathcal{P}^{BB}(\omega,\beta) = \frac{\omega^2}{2c^2}\ \frac{\hbar\omega}{e^{\hbar\omega\beta}-1}. \tag{6}$$

B. The Direct Method of Cavity QED

As noted above, thermal emission is just a form of spontaneous emission — and in the quantum optics and cavity QED community, the modification of spontaneous emission by cavities or PBG structures is a well-known effect [10–19].

Theoretically, in the weak-coupling regime, the spontaneous emission rate $\mathcal{W}_{\mathbf{k}}$ into a wave mode $\mathbf{k}$ is given by *Fermi's Golden Rule* [21],

$$\mathcal{W}_{\mathbf{k}}(\mathbf{r},\omega) = 2\pi\,\rho(\omega_{\mathbf{k}})\,\left|\langle i|\,\mathbf{H}_{\mathbf{k}}|\,f\rangle\right|^2, \tag{7}$$

where

$$\mathbf{H}_{\mathbf{k}} = \boldsymbol{\mu}\cdot\,\mathbf{E}_{\mathbf{k}}(\mathbf{r},\omega_{\mathbf{k}}) \tag{8}$$

is the interaction Hamiltonian for a radiating dipole of moment $\boldsymbol{\mu}$, $|i\rangle$ and $|f\rangle$ are the initial and final atomic states, and $\mathbf{r}$ the dipole location. The electromagnetic mode density $\rho(\omega)$, as well as the spatially dependent modal functions $\mathbf{E}(\mathbf{r},\omega)$, must be computed to generate a result — and this amounts to solving the Helmholtz wave eigenvalue equation in an inhomogeneous media [12]. This solution is extremely hard to come by in 2D and 3D calculations [15], and is not exactly a simple matter even in finite 1D structures [14].

The transition rate $\mathcal{W}_{\mathbf{k}}$, Eq. (7), is the time-averaged rate at which a radiating dipole located at a position $\mathbf{r}$ emits electromagnetic energy of frequency $\omega_{\mathbf{k}}$ into a spatial mode $\mathbf{k}$. For a collection of such emitters, with some known frequency spectrum of emission, the rate $\mathcal{W}(\mathbf{r},\omega_{\mathbf{k}})$ can be averaged over position $\mathbf{r}$, spherical angle element $d\Omega_{\mathbf{k}}$, and multiplied by the emitter power spectrum $\mathcal{P}(\omega)$ to obtain the thermal power output into a particular element of solid angle $d\Omega_{\mathbf{k}}$. This approach has been used successfully in studying the spontaneous emission of light-emitting GaAs semiconductor material embedded in a 1D, thin-film, PBG structure [16]. The power spectrum $\mathcal{P}(\omega)$ in this case is just that of the spontaneous emission of the electrically pumped semiconductor material. To calculate the thermal spectrum by this "direct" method, one simply uses the blackbody thermal spectrum $\mathcal{P}(\omega,\beta)$, Eq. (6), instead. However, because of the numerical and theoretical difficulties involved in solving the Helmholtz eigenvalue equation for a general PBG structure, the thin-film, thermal

emissivity community has independently developed a simpler "indirect" method based on *Kirchoff's Law* of detailed balance for thermal equilibrium. This indirect method works well for 1D thin-film structures, and agrees with the more computationally intensive direct calculation in all cases of interest [22]. This indirect method of emission calculation is apparently not well known in the cavity QED community, where the direct method is used almost exclusively [2,11–16]. For that reason, we review it here briefly.

C. The Indirect Method from Kirchoff's Law

Let us consider a multi-layered, thin-film structure and, for simplicity, concern ourselves with the discussion of optical radiation transmission and reflection on-axis, normal to the surfaces, as shown in Fig. 1. Let $\mathscr{T}$ and $\mathscr{R}$ be the real transmittance and reflectance for the film — representing the ratios of transmitted and reflected optical power (Poynting's vector) with respect to an incident flux from the left, normalized to unity. If no absorption (or gain) is present, then conservation of energy requires that $\mathscr{T} + \mathscr{R} = 1$. However, if absorption is present in the layers, then we may define a real absorptance by $\mathscr{A} = 1 - \mathscr{R} - \mathscr{T}$, which is again a statement of conservation of energy. However, from *Kirchoff's Second Law*, we know that the ratio of the thermal emittance $\mathscr{E}$ to the absorptance $\mathscr{A}$ is a constant, independent of the nature of the material — and that that constant is unity when the source is a perfect blackbody [22,23]. Hence, in this case $\mathscr{E} = \mathscr{A}$ and we may write the fundamental equation for calculating the thermal spectral power of a 1D thin film structure, from *Kirchoff's Law*, as

$$\mathscr{E}_{\mathbf{k}}(\omega) = \mathscr{A}_{\mathbf{k}}(\omega) = 1 - \mathscr{R}_{\mathbf{k}}(\omega) - \mathscr{T}_{\mathbf{k}}(\omega), \tag{9}$$

where $\mathscr{E}(\omega)$ has the interpretation as the ratio of the thermal optical power (Poynting's vector) emitted at frequency ω into a spherical-angle element $d\Omega_{\mathbf{k}}$ (by a unit surface area of the thin film), to the power emitted per unit area by a blackbody at the same temperature T.

This analysis is quite well suited for 1D PBG structures, where $\mathscr{E}_{\mathbf{k}}(\omega)$ may be computed rapidly by matrix transfer techniques. Some care must be taken to account for the complex indices of refraction used to model the presence of absorbing dielectric layers — which will emit upon thermal excitation [24,25]. In principle, there is no reason that the method could not be extended to 2D and 3D PBG structures using the higher-dimensional matrix techniques developed by Pendry and co-workers [26]. It would be a simple matter to include absorption in a 2D or 3D matrix transfer code and hence model the directional power emission of an actual higher-dimensional PBG.

Once the emittance $\mathscr{E}_{\mathbf{k}}(\omega)$, Eq. (9), is obtained, then multiplication by the Planck power spectrum, Eq. (6), gives the power spectrum of the thin-film emitter $\mathscr{P}^{TF}$ in terms of the thin-film emittance $\mathscr{E}_{\mathbf{k}}^{TF}(\omega)$, and the black-body spectrum $\mathscr{P}^{BB}(\omega)$,

$$\mathscr{P}_{\mathbf{k}}^{\mathrm{TF}}(\omega,\beta) = \mathscr{E}_{\mathbf{k}}^{\mathrm{TF}}(\omega)\, \mathscr{P}^{\mathrm{BB}}(\omega), \tag{10}$$

which can then be compared directly to experiment.

In the next section, we show how matrix transfer techniques can be used to compute the on-axis, thin-film, PBG power spectrum, appropriate for the qualitative predictions of a 2D or 3D structure in the John-Wang approxi-mation.

III. ON-AXIS EMITTANCE AND THE JOHN-WANG MODEL

One of the difficulties in dealing with the theory of 2D and 3D PBG structures is the computational complexity associated with solving the full, vector, Maxwell-wave, eigenvalue problem in a 2D or 3D inhomogeneous dielectric [9]. Certain Fourier techniques can be used to establish the eigenvalue (dispersion) curves for *infinite* 2D or 3D periodic structures, which possess a high degree of symmetry. For finite structures, some success has been achieved using 2D and 3D matrix transfer [26] and finite-difference techniques [27]. However, these methods are all

computationally intensive, and hence the results lack a certain qualitative level of physical understanding.

A. The John-Wang Model

Early on, S. John and J. Wang proposed a simple qualitative model for an infinite 2D or 3D photonic band-gap structure [10]. This model was extended later by our group to study dispersion, spontaneous emission, and nonlinear effects in *finite* PBG structures [12–14, 28–33]. The basic idea of the model is to assume that there exists a 3D PBG structure whose Brillouin zone (BZ) is perfectly spherical and the same for both degrees of polarization, as shown in Fig. 2. In fact, it was this search for a nearly spherical BZ that motivated the early experimental work of Yablonovitch [8,9]. The analogous model in 2D is a structure whose BZ is circular and the same for both polarization degrees of freedom. In both cases, this approximation is essentially equivalent to saying that the electromagnetic wave "sees" the same periodic potential — regardless of its polarization or direction of propagation through the PBG. This approximation means that the same 1D periodic potential is seen by all propagating modes, and so the problem reduces to solving the 1D wave equation. This 1D problem may be attacked by analytical methods or simple 1D matrix transfer techniques. In either case, the quantitative on-axis emission spectra of finite, 1D, PBG thin-film stacks, corresponds qualitatively to the 2D or 3D homogeneous emission of the hypothetical John-Wang structure, Fig. 2. The approximation is equivalent to assuming that the band structure does not change much for differing orientations of the photonic crystal.

To begin then, we calculate the on-axis emittance and thermal spectrum of a 1D, thin-film stack, Fig. 1. The results should give a qualitative indication of the omni-directional thermal power spectrum properties of 2D and 3D structures

which have on the order of the same lattice spacing and unit cell size as the 1D stack.

B. Thermal Power Spectrum from Matrix Transfer

The basic model we shall use is illustrated in Fig. 1. We consider light incident from the left in air (index of refraction $n_0 = 1$) onto a 1D, periodic, quarter-wave stack, distributed Bragg reflector (DBR) composed of alternating quarter-wave layers of (possibly) complex indices n_1 and n_2, and of thicknesses a and b, respectively. This DBR photonic band-gap stack is then assumed to be mounted flush on a dielectric substrate of complex index n_3 of thickness d, which is many wavelengths thick at the quarter-wave reference frequency, $\omega_0 = k_0 c = 2\pi c / \lambda_0$, where λ_0 is the quarter-wave reference (midgap) wavelength, and c the vacuum speed of light. Finally, the substrate terminates at the right in air, with index $n_0 = 1$.

In this section, we will consider only the on-axis thermal emission process, leaving angular effects to the next section. Consider again in Fig. 1 that light of unit amplitude is incident from the left. We wish to use matrix transfer techniques [13,14,28–32] to compute the complex transmission and reflection coefficients, $\mathcal{t}$ and $\mathcal{r}$, and the associated transmittance and reflectance, $\mathcal{T} \equiv |\mathcal{t}|^2$ and $\mathcal{R} = |\mathcal{r}|^2$, respectively. The left-hand fields $\mathcal{1}$ and $\mathcal{r}$ are linearly related to the right-hand electric fields $\mathcal{0}$ and $\mathcal{t}$ by

$$\begin{bmatrix} \mathcal{1} \\ \mathcal{r} \end{bmatrix} = \widehat{\mathbf{M}} \begin{bmatrix} \mathcal{t} \\ \mathcal{0} \end{bmatrix} \tag{11}$$

where $\widehat{\mathbf{M}}$ is the two-by-two transfer matrix. From linearity alone, we can conclude that $\widehat{\mathbf{M}}$ must have the form [32],

$$\widehat{\mathbf{M}} = \begin{bmatrix} \mathrm{M}_{11} & \mathrm{M}_{12} \\ \mathrm{M}_{21} & \mathrm{M}_{22} \end{bmatrix} = \begin{bmatrix} 1/\mathcal{t} & \mathrm{M}_{12} \\ \mathcal{r}/\mathcal{t} & \mathrm{M}_{22} \end{bmatrix}. \tag{12}$$

(In the absence of absorption, we can apply time-reversal symmetry to obtain $M_{12} = M_{21}^*$ and $M_{22} = M_{11}^*$, but that symmetry does not hold in the present work where absorption is an integral part of the problem [32].) Hence, once the transfer matrix $\widehat{\mathbf{M}}$ is known, then the electric field transmission and reflection coefficients can be extracted from the elements $\mathcal{t} = 1/M_{11}$ and $\mathcal{r} = \mathcal{t}\, M_{21} = M_{21}/M_{11}$. The Poynting- vector transmittance and reflectance $\mathscr{T}$ and $\mathscr{R}$, describing power flow, are then [23],

$$\mathscr{T} \equiv |\mathcal{t}|^2 = \frac{1}{|\mathrm{M}_{11}|^2}, \tag{13a}$$

$$\mathscr{R} \equiv |\mathcal{r}|^2 = \left|\frac{\mathrm{M}_{21}}{\mathrm{M}_{11}}\right|^2 \tag{13b}$$

with $\mathscr{T} + \mathscr{R} = 1$ only if n_0, n_1, n_2 and n_3 are all real (lossless). When absorption is present, and hence n_1, n_2, or n_3 are complex, $\mathscr{T}$ and $\mathscr{R}$ can be used to give the absorptance $\mathscr{A}$ and emittance $\mathscr{E}$, as per the fundamental equation (9).

For a piecewise constant index profile, such as in Fig. 1, the transfer matrix of the entire stack $\widehat{\mathbf{M}}$ can be decomposed into the product of two elementary matrices $\widehat{\mathbf{\Delta}}_{ij}$ and $\widehat{\mathbf{\Pi}}(p_i)$. The discontinuity matrix $\widehat{\mathbf{\Delta}}_{ij}$ describes the boundary conditions for the transfer of the electric field from left to right across a discontinuous $n_i \rightarrow n_j$ interface, accounting for the Fresnel reflection and transmission coefficients. The propagation matrix $\widehat{\mathbf{\Pi}}(p_i)$ describes free propagation between two interfaces a distance a_i apart in a region of constant index n_i, where

$$\mathrm{p_i} \equiv \mathrm{n_i\, a_i\, \omega/c}\,. \tag{14}$$

These two matrices can be written [13,14,32]

$$\hat{\Delta}_{ij} = \begin{bmatrix} \delta_{ij}^{+} & \delta_{ij}^{-} \\ \delta_{ij}^{-} & \delta_{ij}^{+} \end{bmatrix}, \tag{15a}$$

$$\hat{\Pi}(p_i) = \begin{bmatrix} e^{-ip_i} & 0 \\ 0 & e^{ip_i} \end{bmatrix}, \tag{15b}$$

where

$$\delta_{ij}^{\pm} \equiv \frac{1}{2}\left(1 \pm \frac{n_j}{n_i}\right) \tag{16}$$

are the Fresnel discontinuity coefficients at a n_i to n_j interface. If we now consider the stack of Fig. 1, we can consider the DBR PBG thin-film coating as a repeated unit cell whose transfer matrix is

$$\hat{T} = \hat{\Pi}(p)\ \hat{\Delta}_{12}\,\hat{\Pi}(q)\,\hat{\Delta}_{21}, \tag{17}$$

where we define $p \equiv n_1 a\omega/c$ and $q = n_2 b\omega/c$. If the PBG coating is N periods thick, then the transfer matrix for the entire stack, Fig. 1, is

$$\hat{M} = \hat{\Delta}_{01}\,\hat{T}^{N}\,\hat{\Delta}_{23}\,\hat{\Pi}(s)\,\hat{\Delta}_{30}, \tag{18}$$

where $s \equiv n_3 d\omega/c$, for a substrate of thickness d. If n_0, n_1, n_2, and n_3 are real, then relatively simple analytical expressions for the matrix elements M_{ij}, Eq. (12), can be given [13,14,32]. However, since we are only interested in the cases where at least one of these indices is complex, we will carry out the matrix multiplication numerically, to obtain $\hat{M}$ as a function of n_0, n_1, n_2, n_3, a, b, d, N, and ω. Then the transmittance and reflectance coefficients $\mathscr{T}$ and $\mathscr{R}$ are given by Eq. (13), with the emittance $\mathscr{E}$ obtained therefrom by the fundamental equation (9).

C. Simple Quarter-Wave Stack

We now compute and plot the emittance $\mathscr{E}(\omega)$, Eq. (9), by the indirect method outlined above for the quarter-wave stack of Fig. 1. The first set of plots in Fig. 3 shows the emittance when only the substrate contains absorbers, so we take $n_0 = 1$, $n_1 = \sqrt{2}$, $n_2 = 2$, and $n_3 = 3 + 0.03i$. The substrate is very thick, with $d >> \lambda_0$. Recall

that at a given frequency $\omega = 2\pi c/\lambda$, a complex index $n = n' + in''$ implies an absorption per unit length of

$$\alpha = \frac{4\pi n''}{\lambda} = \frac{2n''\omega}{c}, \tag{19}$$

so that the intensity falls to $1/e$ in the *Beer's Law* distance $1/\alpha$. Note that the absorptance, thence, increases linearly with increasing frequency. For the rest of this work we make the quarter-wave assumption for the thin-film layers, namely $n_1'a = n_2'b = \lambda_0/4$, where $\omega_0 = 2\pi c/\lambda_0$ is the midgap reference frequency of the PBG, for which reflection is maximum. We define $n_1' = \mathrm{Re}\{n_1\}$ and $n_2' = \mathrm{Re}\{n_2\}$. Hence, the real phase factors become $\mathrm{Re}\{p\} = n_1' a\omega/c = \mathrm{Re}\{q\} = n_2' b\omega/c = \pi\omega/(2\omega_0)$, showing that a quarter-wave of phase $\pi/2$ is accumulated whenever $\omega = \omega_0$. We take the substrate thickness d to be many optical wavelengths, $d = 100\,\lambda_0/n_3'$, to model a very thick substrate.

1. *PBG as a passive filter*

In Fig. 3, we show the emissivity $\mathscr{E}$ as a function of the scaled frequency ω/ω_0. With only the substrate index $n_3 = 3 + 0.03i$ complex, this models the situation where a lossless 3D PBG sits atop a heated hotplate (substrate). In this case, the PBG coating acts as a passive filter — blocking heat radiation emitted by the substrate at band-gap frequencies from reaching the left-most n_0 region. We illustrate the effect with $N = 1$, 3, and 5 periods in the PBG, in Figs. 1a, 1b, and 1c, respectively. The dotted line at $\mathscr{E} = 1$ corresponds to the emittance of a perfect blackbody. However, the thick substrate of relatively high index $n_3' = 3$, is not a true blackbody. Even though the substrate is highly absorptive, not all radiation incident from the left — in the absence of the PBG thin film — would be absorbed. This is because the $n_0 \rightarrow n_3$ interface is highly reflective, with a reflection coefficient given by

$$R_{03} = \left| \frac{n_0 - n_3}{n_0 + n_3} \right|^2 , \tag{20}$$

which is $R_{03} \cong 0.25$, for $n_0 = 1$ and $n_3 = 3 + 0.03i$. Hence, the uncoated, absorptive substrate alone, when heated, does not emit as efficiently as a perfect blackbody — but only 75% as efficiently. This so-called "grey-body" emittance of $\mathscr{E} \cong 0.75$ is plotted as a dashed line in Fig. 3.

So now we see an interesting effect. The PBG-coated, heated substrate emits poorly in the band gap, as was expected, and as is clearly shown in Fig. 3. The emission inhibition or filtering becomes more pronounced as the number of periods N is increased and the gap thereby deepens. What is a bit surprising is that, at the photonic pass-band transmission resonances [13,32], the substrate's emission is *enhanced* from the grey-body level all the way up to the perfect blackbody rate. This occurs because the transmission resonances correspond to frequencies at which the PBG thin-film stack acts as an *anti*-reflective coating — eliminating the n_0 to n_3 impedance mismatch seen by the substrate alone. Since all incident radiation from the left at these select frequencies "tunnels" through the PBG into the substrate — all of the power is consequently absorbed and the entire structure behaves then as a blackbody — which is, of course, defined as an object that absorbs all incident radiation.

So, in summary, the results of Fig. 3 illustrate that a passive, lossless PBG coating can inhibit the thermal emittance of a substrate at band-gap frequencies — but enhance it at band-edge transmission resonance frequencies. This result applies quantitatively to the on-axis emissivity of an actual 1D thin-film structure. However, as per the John-Wang model — this result tells us *qualitatively* what to expect at all angles for a 3D PBG mounted on a heated substrate.

2. *PBG as active emitter*

In Fig. 3, all of the absorbers (emitters) were placed in the substrate, as indicated by the shaded region of the inset, and the PBG coating acted as a passive filter. In the next set of plots, Figs. 4 and 5, we move the emitters from the substrate into the PBG itself, where active enhancement and suppression of the thermal emission process occurs, due to the PBG-altered electromagnetic mode structure [12–16]. We expect different effects, depending on whether the emitters are localized in the low-index n_1 or high-index n_2 regions, Figs. 4 and 5, respectively. In particular, it is well known that low-frequency band-edge resonance — at about $\omega/\omega_0 \cong 0.75$ here — occurs when the normal-mode field at that frequency has intensity anti-nodes localized in only the high-index n_2 layers. The situation is reversed at the high-frequency band edge, here at $\omega/\omega_0 \cong 1.25$, where the field-mode intensity maxima are localized in the low-index n_1 layers [9].

This band-edge enhancement phenomenon manifests itself in the emission process. If emitters are doped into the low-index n_1 layers, then they will couple maximally to the high-frequency band-edge resonance modes, as per *Fermi's Golden Rule*, Eq. (7). Thermal emission will thus be enhanced most at this high-frequency band edge, as seen in Fig. 4. The opposite occurs when the emitters are switched over to the high-index n_2 layers, where now emission enhancement is expected to be most pronounced at the low-frequency band-edge resonance, as seen in Fig. 5. These effects have been seen before experimentally by our group in an electrically pumped emitting region within a 1D quarter-wave stack [16]. In that case, the emittance was computed theoretically by the direct method, involving explicit calculation of the eigenmodes for *Fermi's Golden Rule*, Eq. (7). In this current work, we use the indirect method — appropriate for emitters in thermal equilibrium — and we see the same type of results.

In Fig. 4, we take $n_0 = 1$, $n_1 = \sqrt{2} + i\sqrt{2}/100$, $n_2 = 2$, and $n_3 = 1$, so that only the low-index n_1 layers, in the free-standing PBG thin film, are emissive. The plots of Fig. 4 show that, as we increase the number of periods $N \in \{1,3,5\}$, the active emission is suppressed in the gap and enhanced at the edges — with the most pronounced enhancement at the high-frequency band edge, as was predicted.

The curves slope upward to the right due to the fact that the assumed dispersionless imaginary index n_i'', from Eq. (19), implies an absorption per-unit-length that increases linearly with increasing frequency. (This slope did not appear in the emittance curves for the complex n_3, with absorbers only in the substrate, Fig. 3, because there the substrate is taken so thick that all incident radiation entering it is eventually absorbed, regardless of frequency.)

The plot in Fig. 5 shows the emission when the absorbers are swapped from the low- to high-index layers, with $n_1 = \sqrt{2}$, $n_2 = 2 + 0.02i$, and $n_3 = 1$. The emission is suppressed at band-gap frequencies, as before, but the most pronounced enhancement occurs at the low-frequency band-edge, as expected.

In summary then, we expect a passive PBG filter or coating to suppress and enhance the thermal power spectrum of an object in the band gap, as illustrated in Fig. 3. This result applies qualitatively at all angles to the emission filtering with a 3D PBG coating and gives exact quantitative predictors for on-axis emittance measurements using a 1D thin film. In Figs. 4 and 5, we show how the emittance is altered by placing the thermal emitters inside the PBG.

D. Absolute Thermal Power Spectrum

The emittance $\mathscr{E}_{\mathbf{k}}(\omega)$ we have computed so far gives the relative power emitted at each frequency with respect to a perfect black-body emitter. To find the absolute thin-film (TF) power spectrum emitted, $\mathscr{P}_{\mathbf{k}}^{TF}$ as measured by a distant

detector, we need to multiply the thin-film emissivity $\mathscr{E}_k^{TF}$ by the Planck blackbody (BB) power spectrum $\mathscr{P}^{BB}(\omega, T)$, as per Eqs. (6) and (10).

1. *Properties of the Planck spectrum*

The Planck spectrum $\mathscr{P}^{BB}(\omega,T)$, Eq. (6), can be differentiated to find the location of the thermal maximum $\omega_{max}(T)$, which is

$$\omega_{max}(T) = \frac{\left[3 + \mathcal{W}\left(-3e^{-3}\right)\right] k_B T}{\hbar} \cong \frac{2.82\, k_B T}{\hbar}, \tag{21}$$

where $\mathcal{W}(z)$ is the "product log" function [35], which gives the solution for w as a function of z in the transcendental equation $z = w\, e^w$. Then the actual maximum value taken on by the Planck spectrum at this frequency is

$$\mathscr{P}^{BB}_{max}(T) = \mathscr{P}^{BB}(\omega_{max}) \cong \frac{0.71}{\hbar^2 c^2} (k_B T)^3, \tag{22}$$

which illustrates the well-known fact that the maximum power increases cubically with temperature. To scale this absolute maximum out, we normalize by this peak power to get the scaled blackbody spectrum

$$\mathscr{P}^{BB}(\omega,T) = \frac{\mathscr{P}^{BB}(\omega,T)}{\mathscr{P}_{max}(T)} \cong \left(\frac{\hbar\omega}{k_B T}\right)^3 \frac{0.70}{\exp(\hbar\omega/k_B T) - 1}, \tag{23}$$

which, of course, now always has a maximum of unity, by design. The thin-film, normalized power spectrum is easily seen to be the product $\mathscr{P}^{TF} = \mathscr{E}^{TF}\, \mathscr{P}^{BB}$.

2. *Thin-film thermal spectrum*

Now we take the emittance curves, Eq. (9), for the passive PBG coating, Fig. 3, and multiply by the normalized thermal power spectrum, Eq. (23), as per Eq. (10). This gives us the set of plots in Fig. 6. Depending on the temperature T, the maximum of the Planck spectrum can be made coincident with the low-frequency band edge, the high-frequency band edge, or the midgap, as illustrated in Figs. 6a, 6b, and 6c, respectively. The blackbody temperature is, of course,

scaled to the midgap frequency ω_0, via Eq. (21). For example, if the Planck spectrum peaks at midgap, then from Eq. (21) we have the condition on the midgap (MG) temperature T^{MG},

$$\hbar\omega_0 \equiv 2.82\, k_B T^{MG}, \tag{24}$$

which allows us to relate the figures to an absolute temperature scale, T, and the geometric lattice parameters, a, b, n'_1, and n'_2, as per the quarter-wave stack condition

$$n'_1 a = n'_2 b = \frac{\lambda_0}{4} = \frac{\pi c}{2\omega_0}, \tag{25}$$

where $n'_i \equiv \mathrm{Re}\{n_i\}$, as before.

In Fig. 6, we use the same passive filter parameters as before, namely, $n_0 = 1$, $n_1 = \sqrt{2}$, $n_2 = 2$, and $n_3 = 3 + 0.03i$. The solid curves are the normalized power spectra $\mathcal{A}(\omega,T)$, Eq. (23). The dotted lines are the spectra of a perfect blackbody, while the dashed lines are the spectra of the uncoated, high-index ($n'_3 = 3$) substrate (greybody). We see in Figs. 6a and 6b, that the power radiated by the substrate is enhanced when the temperature T is such that the Planck peak aligns with either the low- or high-frequency band edges, respectively. In Fig. 6c, we see thermal emission suppression when the temperature choice aligns the Planck peak with the midgap frequency, ω_0.

In Figs. 7 and 8, we again move the emitters from the substrate into the PBG coating and take $n_3 = 1$, leaving a free-standing absorbing (emitting) DBR grating. In Fig. 7, we have $n_0 = 1$, $n_1 = \sqrt{2} + i\sqrt{2}/100$, $n_2 = 2$, and $n_3 = 1$. The Planck peaks are located at the low-, high-, and midgap frequencies in Figs. 7a, 7b, and 7c, respectively. Since the emitters are in the low-index layers, there is a preference toward emission enhancement at the high-frequency band-edge frequency. The reverse occurs in Fig. 8, where $n_0 = 1$, $n_1 = \sqrt{2}$, $n_2 = 2 + 0.02i$, and $n_3 = 1$.

IV. OFF-AXIS SPECTRUM

In this section, we calculate the off-axis spectrum of our 1D PBG thin film as a function of incident angle θ_0. We begin with a review of an off-axis matrix transfer formalism suitable for complex indices of refraction.

A. Off-Axis Matrix Transfer for Absorbing Media

The generalization of matrix transfer to include off-axis propagation in absorptionless media can be found in many texts [36–38]. However, when the indices of refraction are complex, some technical subtleties appear [24,25]. For that reason, we review the method carefully here.

The off-axis boundary conditions and propagation phases can be accounted for by simple modifications to the on-axis discontinuity and propagation matrices, $\widehat{\Delta}_{ij}$ and $\widehat{\Pi}(p_i)$, respectively, Eq. (15). As shown in Fig. 9, there are two independent polarization modes to consider, the *s*-polarized TE mode, and the *p*-polarized TM mode. For both *s* and *p* polarization, the phase p_i accumulated as the ray traverses an index n_i slab of thickness a_i, needs to be adjusted by a factor of cos θ_i, which projects out the on-axis component of the wave vector $\mathbf{k}_i$. Hence, Eq. (14) becomes,

$$p_i = n_i a_i \omega \cos \theta_i / c \,, \tag{26}$$

where θ_i is the angle $\mathbf{k}_i$ makes with the normal of the slabs, as shown in Fig. 9. Hence, the propagation matrix $\widehat{\Pi}(p_i)$, Eq. (15b), remains the same with the identification $p_i \rightarrow p_i \cos \theta_i$. However, the discontinuity matrix $\widehat{\Delta}_{ij}$, Eq. (15a), takes on two different forms for the *s* and *p* polarizations, reflecting the different boundary conditions on TE versus TM modes at the $n_i \rightarrow n_j$ interface. The form of Eq. (15a) remains the same, with the identification that $\delta_{ij}^{\pm} \rightarrow \delta_{ij}^{s\pm}$ or $\delta_{ij}^{p\pm}$, for TE (*s*-polarized) or TM (*p*-polarized) modes, respectively, where we define

$$\delta_{ij}^{s\pm} \equiv \frac{1}{2}\left(1 \pm \frac{n_j \cos\theta_j}{n_i \cos\theta_i}\right), \tag{27a}$$

$$\delta_{ij}^{p\pm} \equiv \frac{1}{2}\left(1 \pm \frac{n_i \cos\theta_j}{n_j \cos\theta_i}\right). \tag{27b}$$

All that remains is to establish a relationship between the angle of incidence θ_i in an arbitrary layer, n_i, with the measured angle of incidence θ_0 from the left-most semi-infinite medium of index n_0, Fig. 9. This is just given implicitly in the i^{th} layer by Snell's law [25],

$$n_0 \sin\theta_0 = n_i \sin\theta_i . \tag{28}$$

Hence, Eqs. (15), (26), and (27) provide a complete set of matrices for the off-axis problem. The same formalism holds, independently of whether the n_i are complex or not [24,25]. However, in general, when n_i is complex then the associated quantity θ_i is also complex, and it can no longer be interpreted as the physical angle. In this case, which we are concerned with here, the formalism becomes merely a bookkeeping device that tracks the angular dependence of the power flow from left-to-right across the structure.

B. Off-axis Spectrum for Standard 1D Thin Films

In this section, we compute the off-axis emittance for the thin-film parameters considered in the previous sections. First, let us consider the case when the substrate index n_3 is complex, but n_1 and n_2 are real, so that the PBG thin-film coating in Fig. 1 acts as a passive filter. We take $n_0 = 1$, $n_1 = \sqrt{2}$, $n_2 = 2$, and $n_3 = 3 + 0.03i$. It is instructive to plot the emittance $\mathscr{E}(\omega,\theta_0)$ as a three-dimensional surface plot, which shows how the band gap shifts for changing θ_0. We do this in Fig. 10, where we plot the s-polarized, p-polarized, and unpolarized emittances $\mathscr{E}^s(\omega,\theta_0)$, $\mathscr{E}^p(\omega,\theta_0)$, and $\mathscr{E}^u(\omega,\theta_0)$, respectively in (a), (b), and (c). Here, $\mathscr{E}^u \equiv (\mathscr{E}^s + \mathscr{E}^P)/2$, since for unpolarized emitters either polarization mode is

equally likely to be occupied. We see in Fig. 10 that the *s*-gap and *p*-gap both shift from the same gap to different higher frequency gaps as the incident angle θ_0 ranges from *0* to $\pi/2$. The *s*-gap remains deep and wide, whereas the *p*-gap tends to narrow and fill in. In particular, the *p* midgap at $\theta_0 \cong 0$ shifts to the low-frequency *p*-band-edge resonance, near $\theta_0 \cong \pi/2$, Fig. 10b. This means that the thin film has a very low emittance on-axis, but a high value at large angles off-axis. The width of the gap $\Delta\omega_0$ at $\theta_0 = 0$ is determined solely by the material parameters $n'_1 \equiv \mathrm{Re}\{n_1\}$ and $n'_2 \equiv \mathrm{Re}\{n_2\}$, via [32, 36, 37]

$$\frac{\Delta\omega}{\omega_0} = \frac{4}{\pi} \arcsin\left(\frac{n'_2 - n'_1}{n'_2 + n'_1}\right) \cong \frac{2}{\pi} \frac{\Delta n}{\bar{n}}, \tag{29}$$

where $\Delta n = n_2 - n_1$ and $\bar{n} = (n_1 + n_2)/2$. (The approximation holds for $\Delta n/\bar{n} << 1$.)

Note in Fig. 10 that both the *s* and *p* emittance drops to zero at all frequencies as $\theta_0 \rightarrow \pi/2$. This is because the PBG coating can only modulate the basic Lambertian emission angular dependence, which is proportional to $\cos^2\theta_0$. Hence the emittance vanishes as $\theta_0 \rightarrow \pi/2$, regardless of frequency.

For completeness, we now consider the case of a free-standing PBG with absorbers (emitters) in the n_1 or n_2 layers, with $n_3 = n_0$. In Fig. 11, we take $n_0 = n_3 = 1$, $n_1 = \sqrt{2} + i\sqrt{2}/100$, and $n_2 = 2$. We see that the *s*-polarized and *p*-polarized emittance are modulated slightly differently, in Figs. 11a and 11b, respectively. Both curves show marked emittance resonances at the high-frequency band edge and relatively large angles off-axis. The unpolarized angular spectrum is shown in Fig. 11c. Similarly, in Fig. 12, we take $n_0 = n_3 = 1$, $n_1 = \sqrt{2}$, and $n_2 = 2 + 0.02i$. We see similar effects as in Fig. 11, but now with the larger emission resonances at the low-frequency side of the gap.

V. SUMMARY AND CONCLUSIONS

In this paper, we have tried to give a general discussion of the theory of thermal power-spectrum modification in 1D, periodic, photonic band-gap structures. The theory applies qualitatively to 2D and 3D photonic band-gap materials, within the John-Wang approximation. The 1D thermal spectrum calculations should easily be extendable to the 2D and 3D matrix transfer method of Pendry [26], applicable to higher-dimensional PBG structures. We also present a formalism for computing the off-axis thermal spectrum, which gives quantitative results which are directly comparable to experiment.

ACKNOWLEDGEMENTS

We would like to acknowledge interesting and useful discussions with M. J. Bloemer, H. O. Everitt, M. Scalora, A. M. Steinberg, P. A. M. Steinberg, and J. E. Sipe.

REFERENCES

* Permanent address: Quantum Computing Group, Mail Stop 126-347, Information and Computing Technologies Research, Section 395, NASA Jet Propulsion Laboratory, California Institute of Technology, 4800 Oak Grove Drive, Pasadena, CA 91109. Electronic address: jonathan.p.dowling@jpl.nasa.gov.

1. E. M. Purcell, Phys. Rev. **69**, 681 (1947).
2. G. Barton, Proc. R. Soc. London, Ser. A **320**, 251 (1970); P. W. Milonni and P. L. Knight, Opt. Commun. **9**, 119 (1973); G. S. Agarwal, Phys. Rev. A **24**, 2889 (1981); A. O. Barut and J. P. Dowling, Phys. Rev. A **36**, 649 (1987); W. Jhe *et al.*, Phys. Rev. Lett. **58**, 666 (1987); W. Jhe, Phys. Rev. A **44**, 5932 (1991).
3. D. Meschede, H. Walther, and G. Müller, Phys. Rev. Lett. **54**, 551 (1985); R. G. Hulet, E. S. Hilfer, and D. Kleppner, *ibid.* **55**, 2137 (1985); F. DeMartini *et al.*, *ibid.* **59**, 2955 (1987); H. Yokoyama *et al.*, Appl. Phys. Lett. **57**, 2814 (1990); D. G.

Deppe and C. Lei, J. Appl. Phys. **70**, 3443 (1991); G. Björk *et al.*, Phys. Rev. A **44**, 669 (1991); D. L. Huffaker *et al.*, Appl. Phys. Lett. **60**, 3203 (1992).

4. H. G. B. Casimir and D. Polder, Phys. Rev. **73**, 360 (1948); G. Barton, J. Phys. B **7**, 2134 (1974); G. Barton, Proc. Roy. Soc. (London) Ser. A **410**, 141 (1987); A. O. Barut and J. P. Dowling, Phys. Rev. A **36**, 2550 (1987); D. Meschede, W. Jhe, and E. A. Hinds, Phys. Rev. A **41**, 1587 (1990); E. A. Hinds and V. Sandoghdar, Phys. Rev. A **43**, 398 (1991); C. I. Sukenik, *et al.,* Phys. Rev. Lett. **70**, 560 (1993).
5. G. Barton and H. Grotch, J. Phys. A **10**, 1201 (1977); E. Fischbach and N. Nakagawa, Phys. Rev. D **30**, 2356 (1984); M. Kreuzer and K. Svozil, Phys. Rev D **34**, 1429 (1986); L. S. Brown and G. Gabrielse, Rev. Mod. Phys. **58**, 233 (1986); A. O. Barut and J. P. Dowling, Phys. Rev. A **39**, 2796 (1989).
6. J. P. Dowling, Phys. Rev. A **45**, 3121 (1992).
7. F. De Martini, *et al.,* Phys. Rev. A **53**, 471 (1996).
8. E. Yablonovitch, Phys. Rev. Lett. **58**, 2059 (1987); S. John, Phys. Rev. Lett. **58**, 2486 (1987).
9. *Development and Applications of Materials Exhibiting Photonic Band Gaps,* edited by C. M. Bowden, J. P. Dowling, and H. O. Everitt, J. Opt. Soc. Am. B **10** (2) (February, 1993) special issue; *Photonic Band Structures,* edited by G. Kurizki and J. W. Haus, J. Mod. Opt. **41** (2) (February, 1994) special issue; J. D. Joannopoulos, R. D. Meade, and J. N. Winn, *Photonic Crystals: Molding the Flow of Light,* (Princeton University Press, Princeton, 1995); *Photonic Band Gap Materials,* edited by C. M. Soukoulis, (NATO ASI Series, Kluwer Academic Publishers, The Netherlands, 1996); *Microcavities and Photonic Bandgaps: Physics and Applications,* edited by J. Rarity and C. Weisbuch, (NATO ASI Series, Kluwer Academic Publishers, The Netherlands, 1996).
10. S. John and J. Wang, Phys. Rev. Lett. **64**, 2418 (1990); S. John and J. Wang, Phys. Rev. B **43**, 12772 (1991).

11. R. J. Glauber and M. Lewenstein, Phys. Rev. A **43**, 467 (1991).

12. J. P. Dowling and C. M. Bowden, Phys. Rev. A **46**, 612 (1992).

13. J. M. Bendickson, J. P. Dowling, and M. Scalora, Phys. Rev. E. **53**, 4107 (1996).

14. I. S. Fogel, J. M. Bendickson, M. D. Tocci, M. J. Bloemer, M. Scalora, C. M. Bowden, and J. P. Dowling, J. Euro. Opt. Soc. A **7**, 393 (1998).

15. T. Suzuki and P. K. L. Yu, J. Opt. Soc. Am. B **12**, 570 (1995); T. Suzuki, *et al.*, J. Appl. Phys. **79**, 582 (1996).

16. M. Scalora, J. P. Dowling, M. Tocci, M. J. Bloemer, C. M. Bowden, and J. W. Haus, Applied Physics B: Lasers and Optics **60**, Supplements 2-3, S57 (1995); M. D. Tocci, M. Scalora, M. J. Bloemer, J. P. Dowling, and C. M. Bowden, Phys. Rev. A **53**, 2799 (1996).

17. J. P. Dowling and C. M. Bowden, J. Opt. Soc. Am. B **10**, 353 (1993); S. John and T. Quang, Phys. Rev. A **50**, 1764 (1994); S.-Y. Zhu, H. Chen, and H. Huang, Phys. Rev. Lett. **79**, 205 (1997).

18. J. Martorell and N. M. Lawandy, Phys. Rev. Lett. **65**, 1877 (1990); R. Sprik, B. A. Van Tiggelen, and A. Lagendijk, Europhys. Lett. **35**, 265 (1996); S. C. Kitson, W. L. Barnes, and J. R. Sambles, Phys. Rev. Lett. **77**, 2670 (1996); S. Fan, P. R. Villeneuve, and J. D. Joannopoulos, Phys. Rev. Lett. **78**, 3294 (1997); A. Kamli, *et al.,* Phys. Rev. A **55**, 1454 (1997); F. Wijnands, *et al.,* Opt. Quant. Electron. **29**, 199 (1997).

19. E. R. Brown, C. D. Parker, and E. Yablonovitch, J. Opt. Soc. Am. B **10**, 404 (1993); E. R. Brown, C. D. Parker, and O. B. McMahon, Appl. Phys. Lett. **64**, 3345 (1994); K. Agi, *et al.,* Electron. Lett. **30**, 2166 (1994); S. D. Cheng, et al., Appl. Phys. Lett. **67**, 3399 (1995); M. P. Kesler, *et al.,* Microwave Opt. Technol. Lett. **11**, 169 (1996); M. M. Sigalas, R. Biswas, and K.-M. Ho, Microwave Opt. Technol. Lett. **13**, 205 (1996); E. R. Brown, and O. B. McMahon, Appl. Phys. Lett. **68**, 1300 (1996); M. M. Sigalas, *et al.,* Microwave Opt. Technol. Lett. **15**, 153 (1997); G. Poilasne, *et al.,*

Microwave Opt. Technol. Lett. **15**, 384 (1997); H.-Y. D. Yang, N. G. Alexopoulos, and E. Yablonovitch, IEEE Trans. Antennas Propag. **45**, 185 (1997); W. Y. Leung, R. Biswas, and K.-M. Ho, IEEE Trans. Antennas Propag. **45**, 1569 (1997).

20. M. Planck, *The Theory of Heat Radiation* (Dover, New York, 1959); F. K. Richtmyer, E. H. Kennard, and J. N. Cooper, *Introduction to Modern Physics,* 6th ed. (McGraw-Hill, New York, 1969); T. S. Kuhn, *Black-Body Theory and the Quantum Discontinuity, 1894–1912* (University of Chicago Press, Chicago, 1987).
21. E. Merzbacher, *Quantum Mechanics,* 2nd ed. (Wiley, New York, 1970), Ch. 18, Sec. 8.
22. P. Pigeat, D. Rouzel, and B. Weber, Phys. Rev. B **57**, 9293 (1998).
23. J. B. Marion, *Classical Electromagnetic Radiation,* (Academic Press, New York, 1965), Sec. 6.5.
24. M. A. Dupertuis, M. Proctor, and B. Acklin, J. Opt. Soc. Am. A **11**, 1159 (1994); M. A. Dupertuis, B. Acklin, and M. Proctor, J. Opt. Soc. Am. A **11**, 1167 (1994).
25. K. Yamamoto and H. Ishida, Vibrational Spectrosc. **8**, 1 (1994); K. Yamamoto and H. Ishida, Appl. Spectrosc. **48**, 775 (1994); K. Yamamoto, A. Masui, and H. Ishida, Appl. Opt. **33**, 6285 (1994).
26. J. B. Pendry, J. Mod. Optics **41**, 209 (1994); M. M. Sigalas, et al., in *Proceedings of the 1994 SPIE Modeling and Simulation of Laser Systems III,* Vol. 2117, (Society of Photo-Optical Instrumentation Engineers, Bellingham, 1994) pp. 23-31; P. M. Bell, J. B. Pendry, and A. J. Ward, Comp. Phys. Commun. **85**, 306 (1995); J. M. Elson and P. Tran, J. Opt. Soc. Am. A **12**, 1765 (1995); J. M. Elson and P. Tran, Phys. Rev. B **54**, 1711 (1996); J. Chongjun, Q. Bai, and Q. Ruhu, Opt. Commun. **142**, 179 (1997).

27. P. K. Kelly, J. G. Maloney, B. L. Shirley, and R. L. Moore, in *Proceedings of the 1994 IEEE Antennas and Propagation International Symposium,* Vol. 2 (IEEE, Seattle, 1994) pp. 718-721; A. Reineix and B. Jecko, Ann. Telecommun. **51**, 656 (1996); G. Tayeb and D. Maystre, J. Opt. Soc. Am. A **14**, 3323 (1997); H. Y. D. Yang, IEEE Trans. Microwave Theory Tech. **44**, 2688 (1996).

28. M. Scalora, J. P. Dowling, C M. Bowden, and M. J. Bloemer, Phys. Rev. Lett. **73**, 1368 (1994).

29. M. Scalora, J. P. Dowling, M. J. Bloemer, and C. M. Bowden, J. App. Phys. **76**, 2023 (1994); M. D. Tocci, M. J. Bloemer, M. Scalora, J. P. Dowling, and C. M. Bowden, App. Phys. Lett. **66**, 2324 (1995).

30. M. Scalora, M. J. Bloemer, A. S. Manka, J. P. Dowling, C. M. Bowden, R. Viswanathan, and J. W. Haus, Phys. Rev. A **56**, 3166 (1997).

31. M. Scalora, R. J. Flynn, S. B. Reinhardt, R. L. Fork, M. D. Tocci, M. J. Bloemer, C. M. Bowden, H. S. Ledbetter, J. M. Bendickson, J. P. Dowling, and R. P. Leavitt, Phys. Rev. E **54**, R1078 (1996).

32. J. P. Dowling, "Parity, Time-Reversal, and Group Delay for Inhomogeneous Dielectric Slabs: Application to Pulse Propagation in Finite, One-Dimensional, Photonic Band-Gap Structures," submitted to the IEE Proceedings on Optoelectronics, *Special Issue on Photonic Crystals and Photonic Microstructures*, edited by T. Krauss (December 1998).

33. M. Scalora, M. J. Bloemer, A. S. Manka, S. D. Pethel, J. P. Dowling, and C. M. Bowden, J. App. Phys. **84**, 2377 (1998); M. J. Bloemer and M. Scalora, Appl. Phys. Lett. **72**, 1676 (1998).

34. B. Eggleton, R. E. Slusher, C. M. de Sterke, P. A. Krug, and J. E. Sipe, Phys. Rev. Lett. **76**, 1627 (1996).

35. Stephen Wolfram, *The Mathematica Book*, 3rd ed. (Wolfram Media, Cambridge University Press, 1996), Sec. 3.2.10.

36. A. Yariv and P. Yeh, *Optical Waves in Crystals* (Wiley, New York, 1984).

37. P. Yeh, *Optical Waves in Layered Media* (Wiley, New York, 1988).

38. W. C. Chew, *Waves and Fields in Inhomogeneous Media* (Van Nostrand Reinhold, New York, 1990).

FIGURE CAPTIONS

Fig. 1. We indicate the basic photonic band-gap, thin-film coating under investigation for emissivity control. An N-period quarter-wave stack of alternating indices of refraction n_1 and n_2 coats a many-wavelength-thick substrate of index n_3. The entire structure is embedded in a medium, taken to be air, $n_0 = 1$.

Fig. 2. The underlying assumption of the John-Wang approximation is to replace a 2D or 3D PBG structure with an effective 1D model (a). This is equivalent to assuming a 2D or 3D PBG structure with a perfectly circular or spherical Brillouin zone, respectively, for both polarizations (b).

Fig. 3. The emissivity of an absorbing substrate ($n_3 = 3 + 0.03i$) coated by a lossless, PBG thin-film ($n_1 = \sqrt{2}$ and $n_2 = 2$). The solid line is the on-axis emittance $\mathscr{E}(\omega)$, Eq. (9). The dotted line is the emittance of a perfect blackbody substrate, while the dashed line is the actual grey-body emittance of a substrate of index $n_3 = 3 + 0.03i$. We see that the emittance is suppressed in the band gap as a function of the number of periods, N. In the pass bands, the emittance is enhanced all the way to unity at the transmission resonances, where the PBG acts as an anti-reflective coating.

Fig. 4. Here, the substrate is lossless, $n_3 = 1$, and the absorbers are in the absorbing $n_1 = \sqrt{2} + i\sqrt{2}/100$ region, with $n_2 = 2$ lossless. The curve increases linearly overall with ω/ω_0, since a complex $n_1 = n_1' + i\,n_1''$ implies a loss-per-unit length that increases linearly with frequency. The emission enhancement is highest at the high-frequency band edge, where the electric field modes overlap preferentially with the low-index n_1 layers.

Fig. 5. The absorbers are in the high-index $n_2 = 2 + 0.02i$ layers, with $n_1 = \sqrt{2}$ and $n_3 = 1$ lossless. Emission enhancement is now strongest at the low-

frequency band edge, where the field modes overlap predominantly with the high-index n_2 layers.

Fig. 6. The absolute thermal power spectrum with lossless $n_0 = 1$, $n_1 = \sqrt{2}$, $n_2 = 2$, and absorbing $n_3 = 3 + 0.03i$. The temperature is chosen so that the blackbody peak aligns with the low-frequency band edge (a), the high-frequency band edge (b), and midgap (c).

Fig. 7. Same as Fig. 6, but with $n_0 = 1$, $n_1 = \sqrt{2} + i\sqrt{2}/100$, and $n_3 = 1$. Thermal peak is at the low and high band edges and midgap, (a), (b), and (c), respectively. Enhancement is most pronounced at the high-frequency band edge because absorbers are in the low-index n_1 layers.

Fig. 8. Same as Fig. 7, but with absorbers in high-index n_2 layers. Emission is therefore most pronounced at the low-frequency band edge.

Fig. 9. Ray propagation through a multi-layer stack. The incident angle θ_0 from the air on the left is a tunable parameter. Boundary conditions differ for TM waves (p-polarized) and TE waves (s-polarized, out of page).

Fig. 10. Emittance $\mathscr{E}(\omega, \theta_0)$ as a function of stack incident angle θ_0 and scaled frequency ω/ω_0. TE-mode (s-polarized) emittance $\mathscr{E}^s$ is plotted in (a), TM-mode (p-polarized) emittance $\mathscr{E}^p$ in (b), and unpolarized $\mathscr{E}^u = (1/2)(\mathscr{E}^s + \mathscr{E}^p)$ in (c). Here, the substrate is emissive, $n_3 = 3 + 0.03i$, while the PBG coating is $N = 5$ periods thick and lossless, $n_1 = \sqrt{2}$, $n_2 = 2$. Note how the s- and p-gaps shift to higher frequency with increasing θ_0.

Fig. 11. The s-, p-, and unpolarized angular emittance $\mathscr{E}(\omega, \theta_0)$ for an $n_1 = \sqrt{2} + i\sqrt{2}/100$ emissive PBG coating with $n_0 = 1$, $n_2 = 2$, and $n_3 = 1$ lossless.

Fig. 12. Angular emittance $\mathscr{E}(\omega,\theta_0)$, same as Fig. 1, but with absorbers in the high-index $n_2 = 2 + 0.02i$, with $n_0 = 1$, $n_1 = \sqrt{2}$, and $n_3 = 1$.

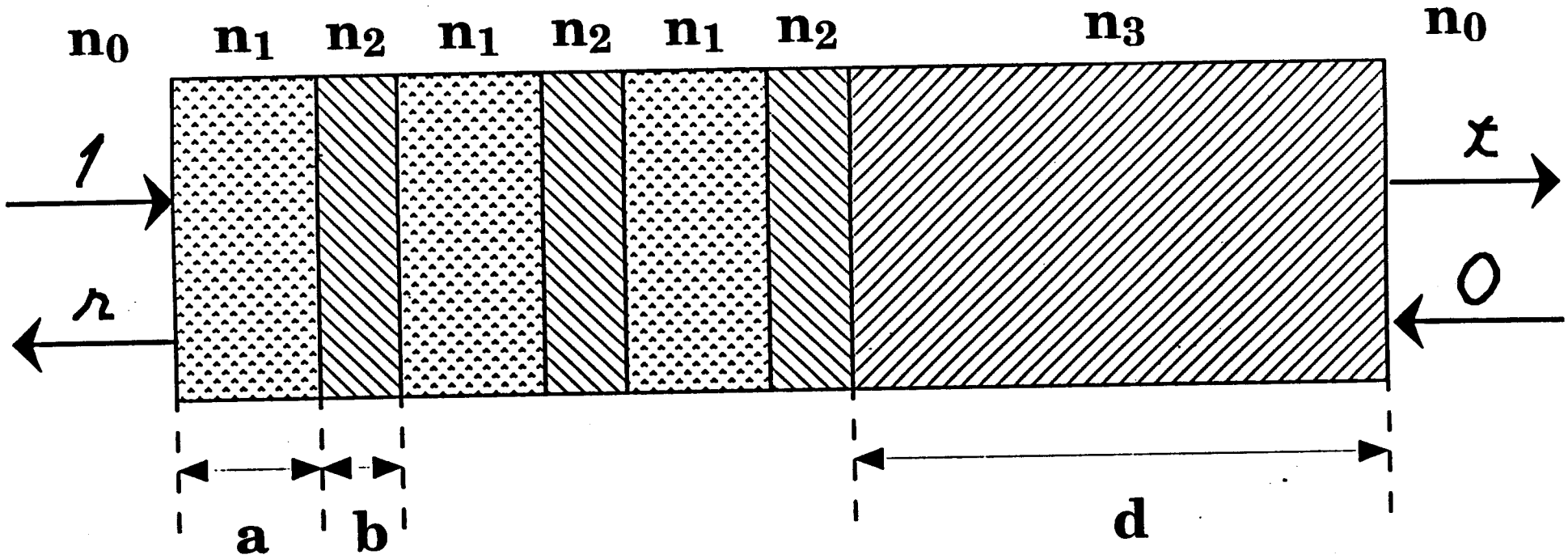

Fig. 1

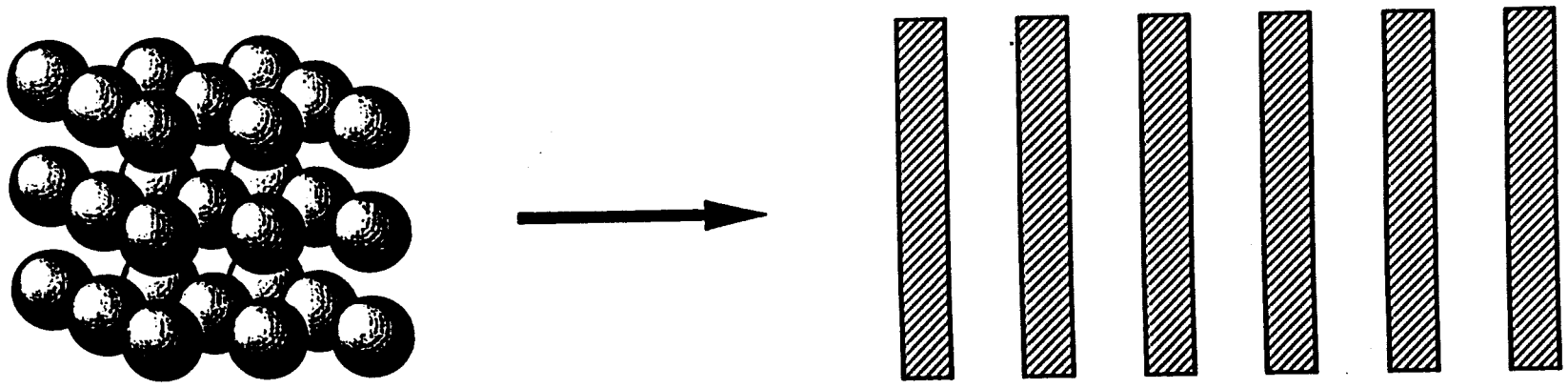

(a)

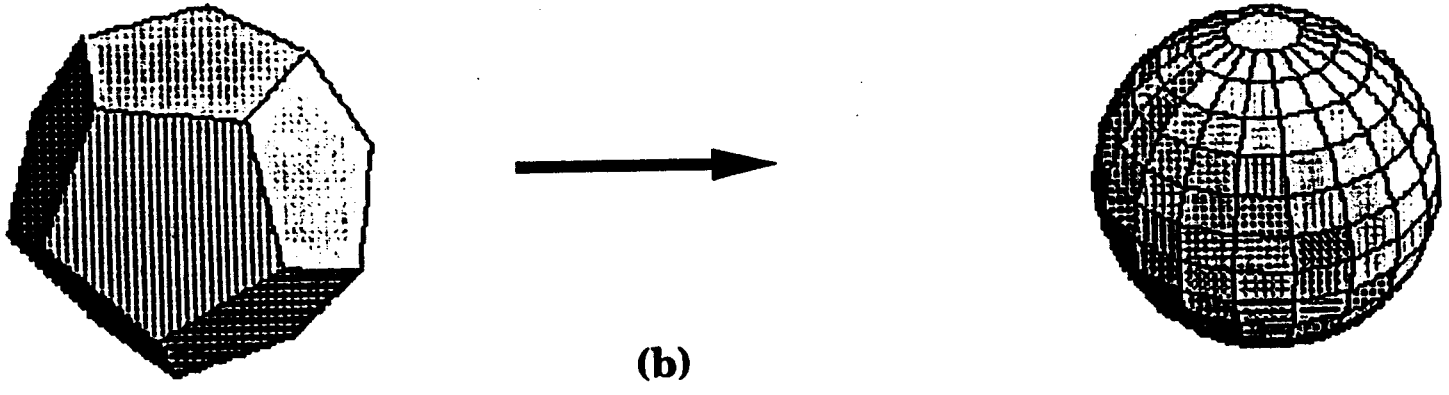

(b)

Fig. 2

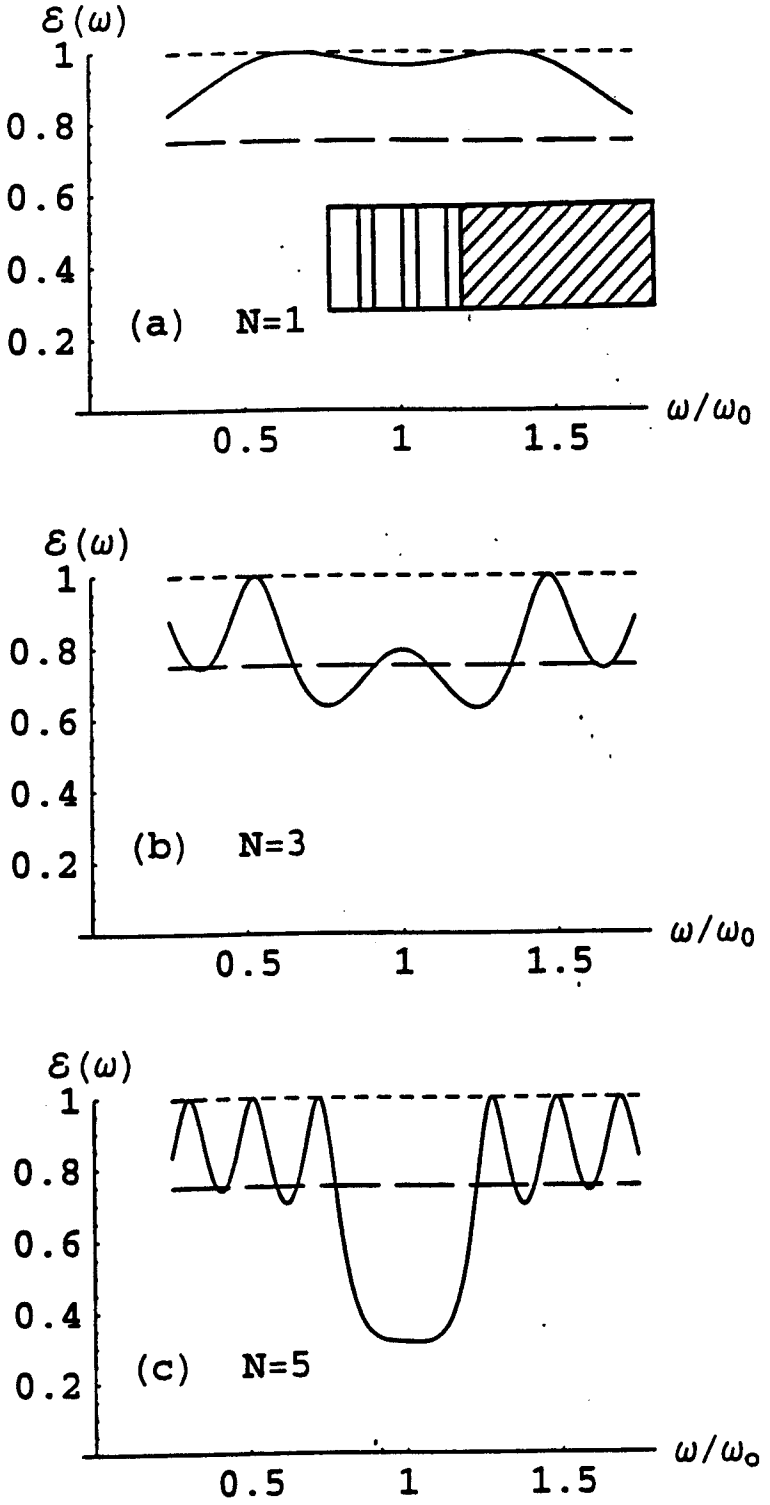
ε(ω)
1
0.8
0.6
0.4
0.2
(a) N=1
ω/ω0
0.5
1
1.5
ε(ω)
1
0.8
0.6
0.4
0.2
(b) N=3
ω/ω0
0.5
1
1.5
ε(ω)
1
0.8
0.6
0.4
0.2
(c) N=5
ω/ω0
0.5
1
1.5

Fig. 3

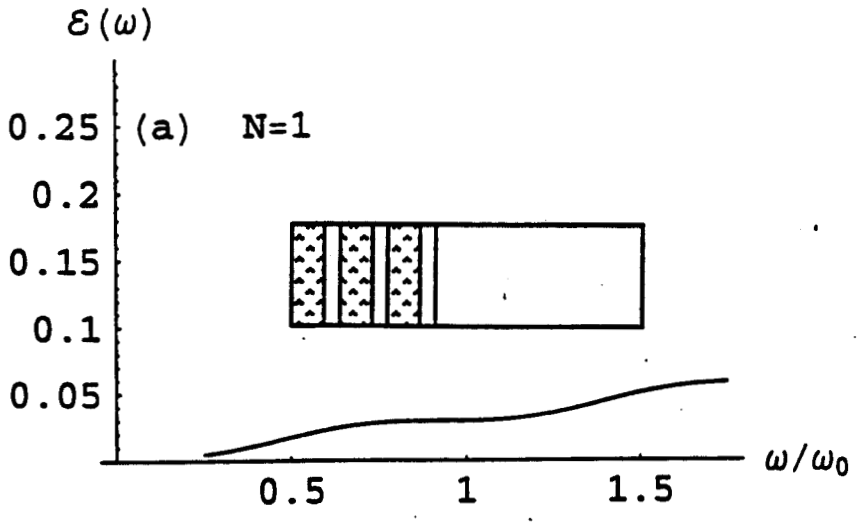
ε(ω)
0.25
(a) N=1
0.2
0.15
0.1
0.05
ω/ω0
0.5
1
1.5

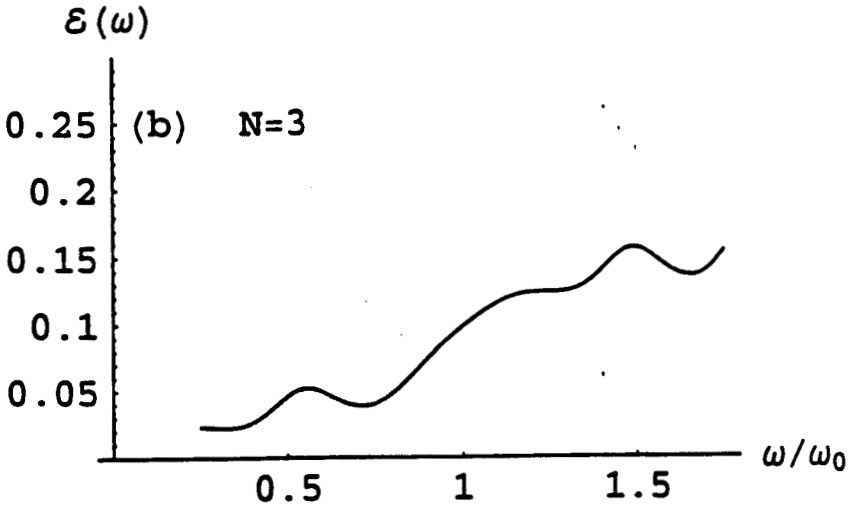
ε(ω)
0.25
(b) N=3
0.2
0.15
0.1
0.05
ω/ω0
0.5
1
1.5

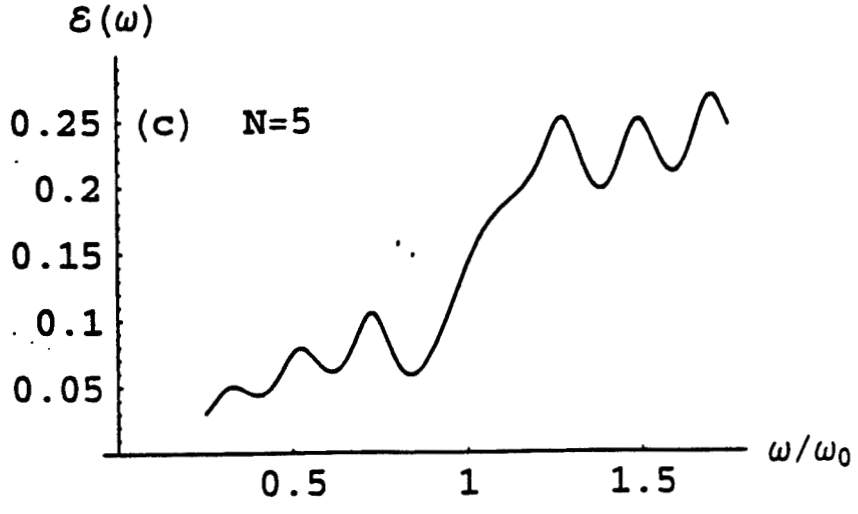
ε(ω)
0.25
(c) N=5
0.2
0.15
0.1
0.05
ω/ω0
0.5
1
1.5

Fig. 4

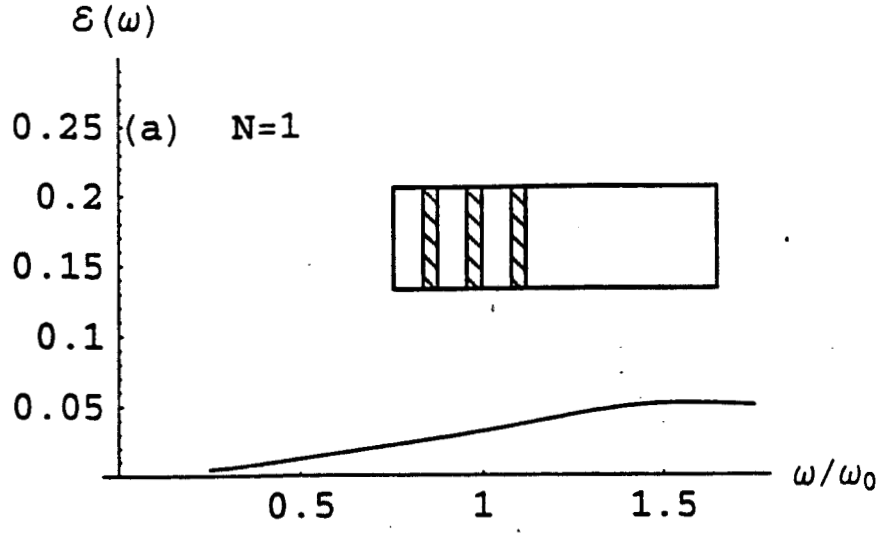
ε(ω)
0.25
(a) N=1
0.2
0.15
0.1
0.05
0.5
1
1.5
ω/ω0

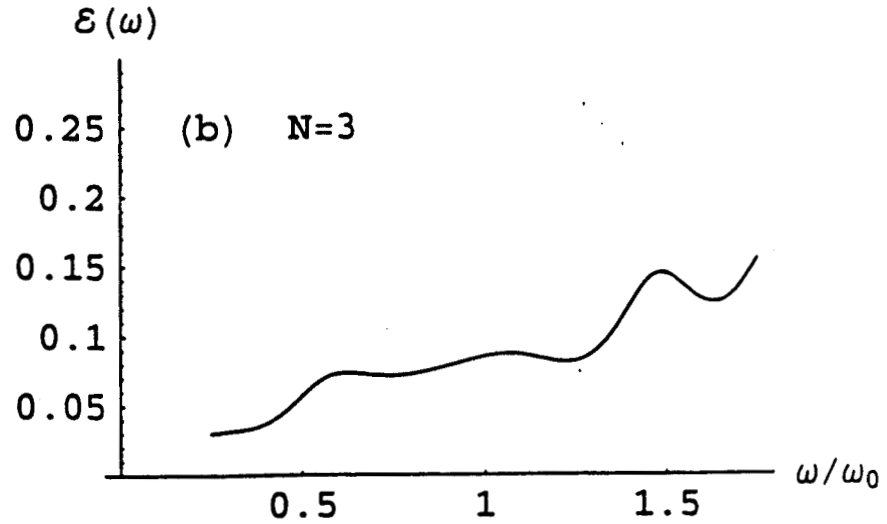
ε(ω)
0.25
(b) N=3
0.2
0.15
0.1
0.05
0.5
1
1.5
ω/ω0

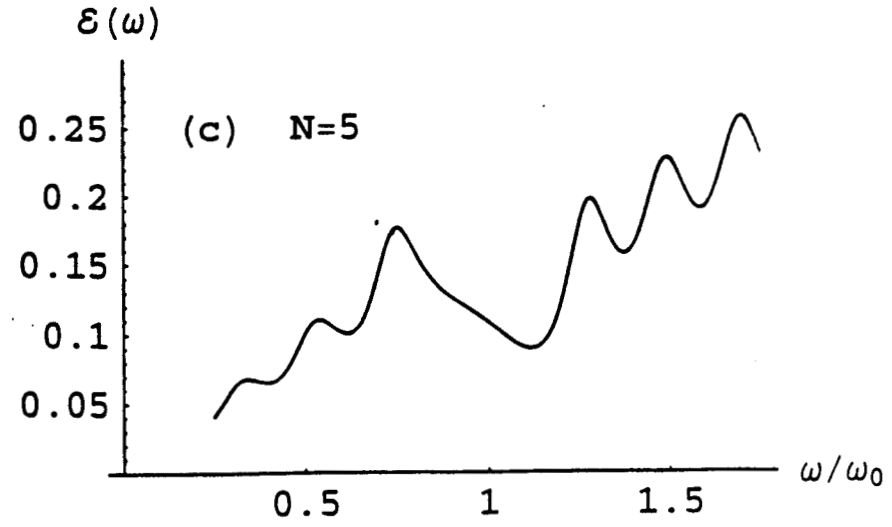
ε(ω)
0.25
(c) N=5
0.2
0.15
0.1
0.05
0.5
1
1.5
ω/ω0

Fig. 5

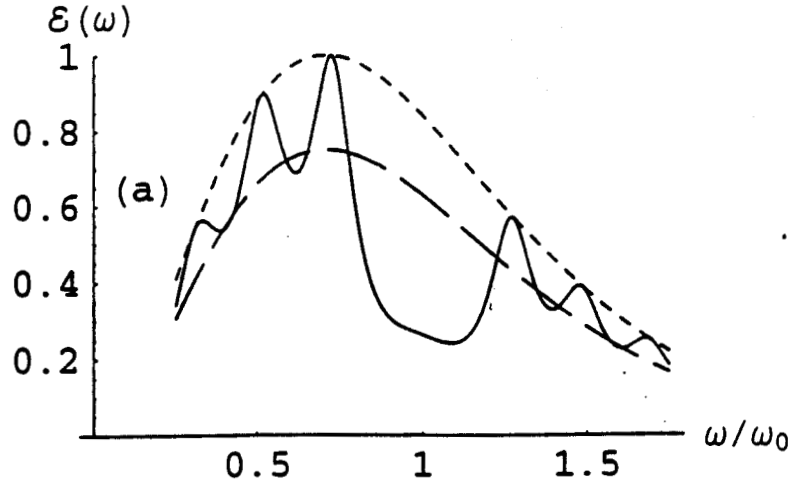
ε(ω)
1
0.8
0.6
0.4
0.2
(a)
0.5
1
1.5
ω/ω0

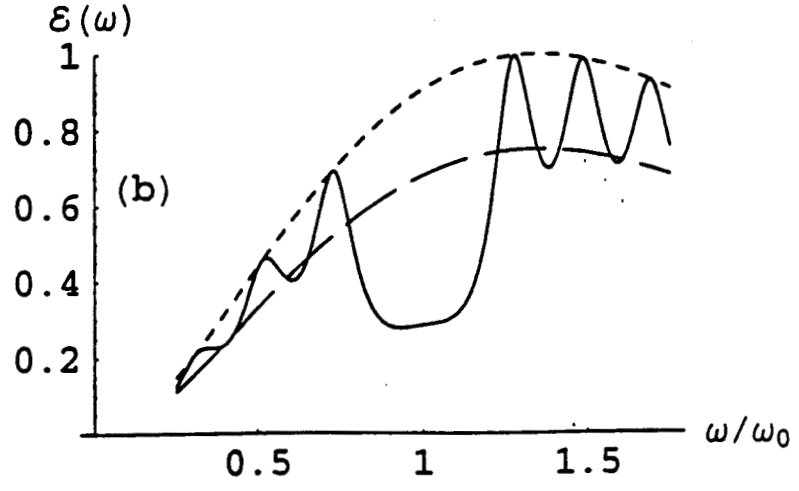
ε(ω)
1
0.8
0.6
0.4
0.2
(b)
0.5
1
1.5
ω/ω0

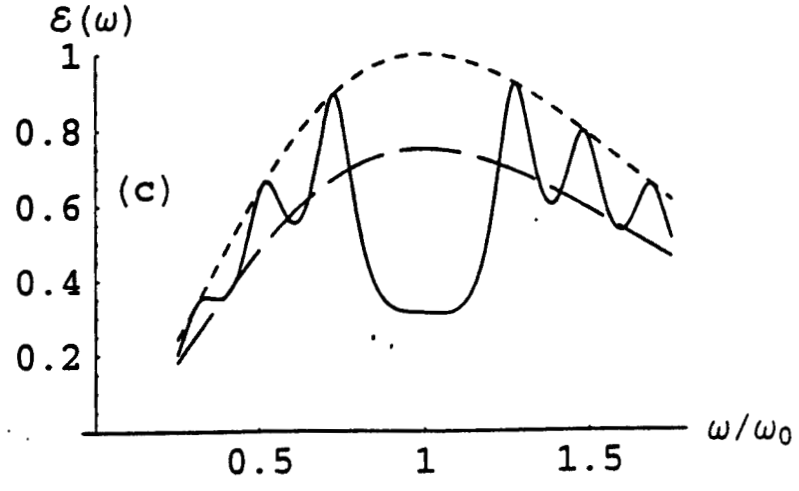
ε(ω)
1
0.8
0.6
0.4
0.2
(c)
0.5
1
1.5
ω/ω0

Fig. 6

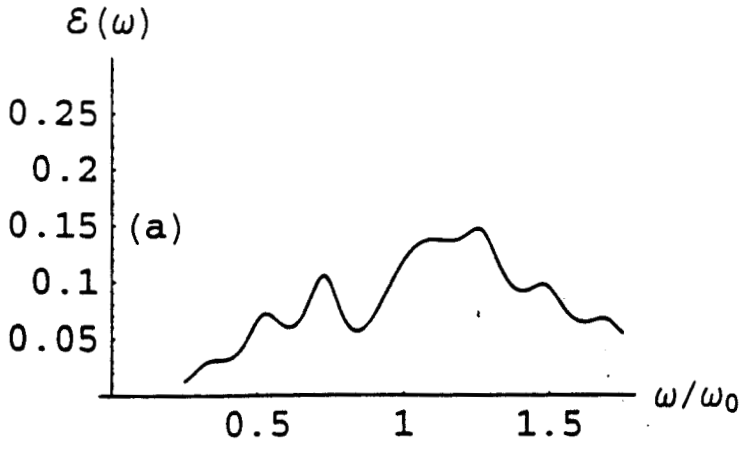
ε(ω)
0.25
0.2
0.15
(a)
0.1
0.05
0.5
1
1.5
ω/ω0

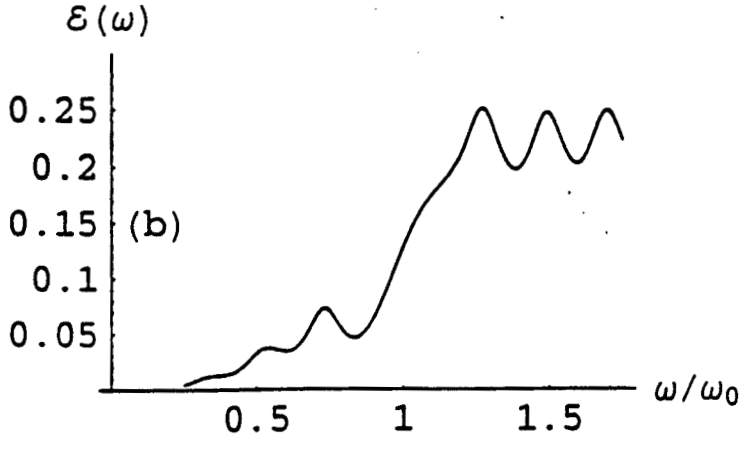
ε(ω)
0.25
0.2
0.15
(b)
0.1
0.05
0.5
1
1.5
ω/ω0

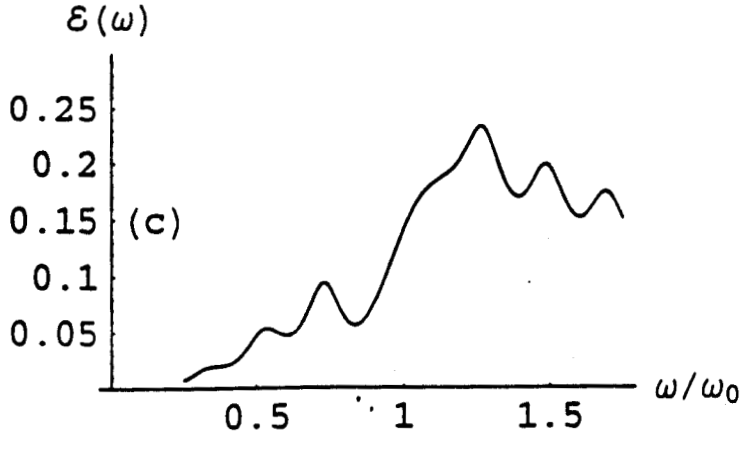
ε(ω)
0.25
0.2
0.15
(c)
0.1
0.05
0.5
1
1.5
ω/ω0

Fig. 7

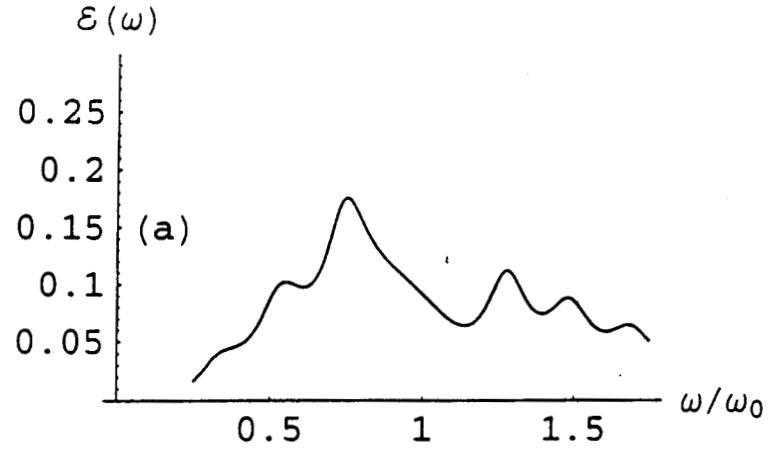
ε(ω)
0.25
0.2
0.15
(a)
0.1
0.05
0.5
1
1.5
ω/ω0

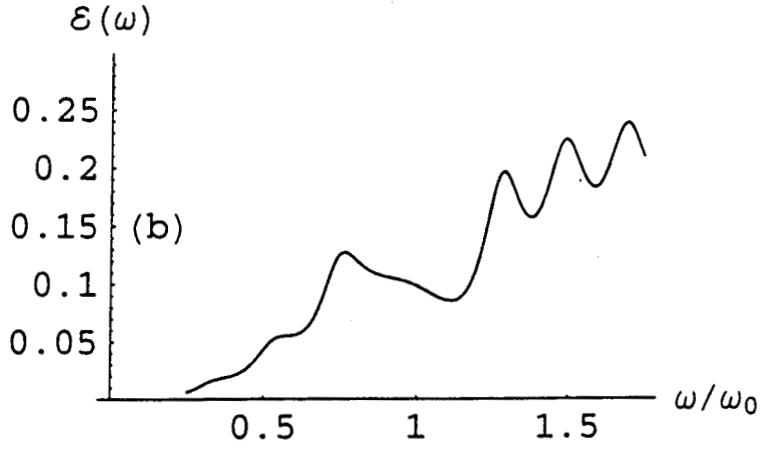
ε(ω)
0.25
0.2
0.15
(b)
0.1
0.05
0.5
1
1.5
ω/ω0

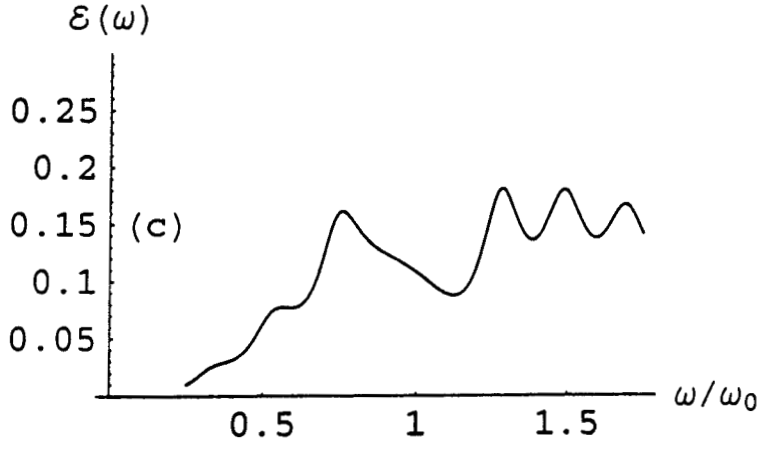
ε(ω)
0.25
0.2
0.15
(c)
0.1
0.05
0.5
1
1.5
ω/ω0

Fig. 8

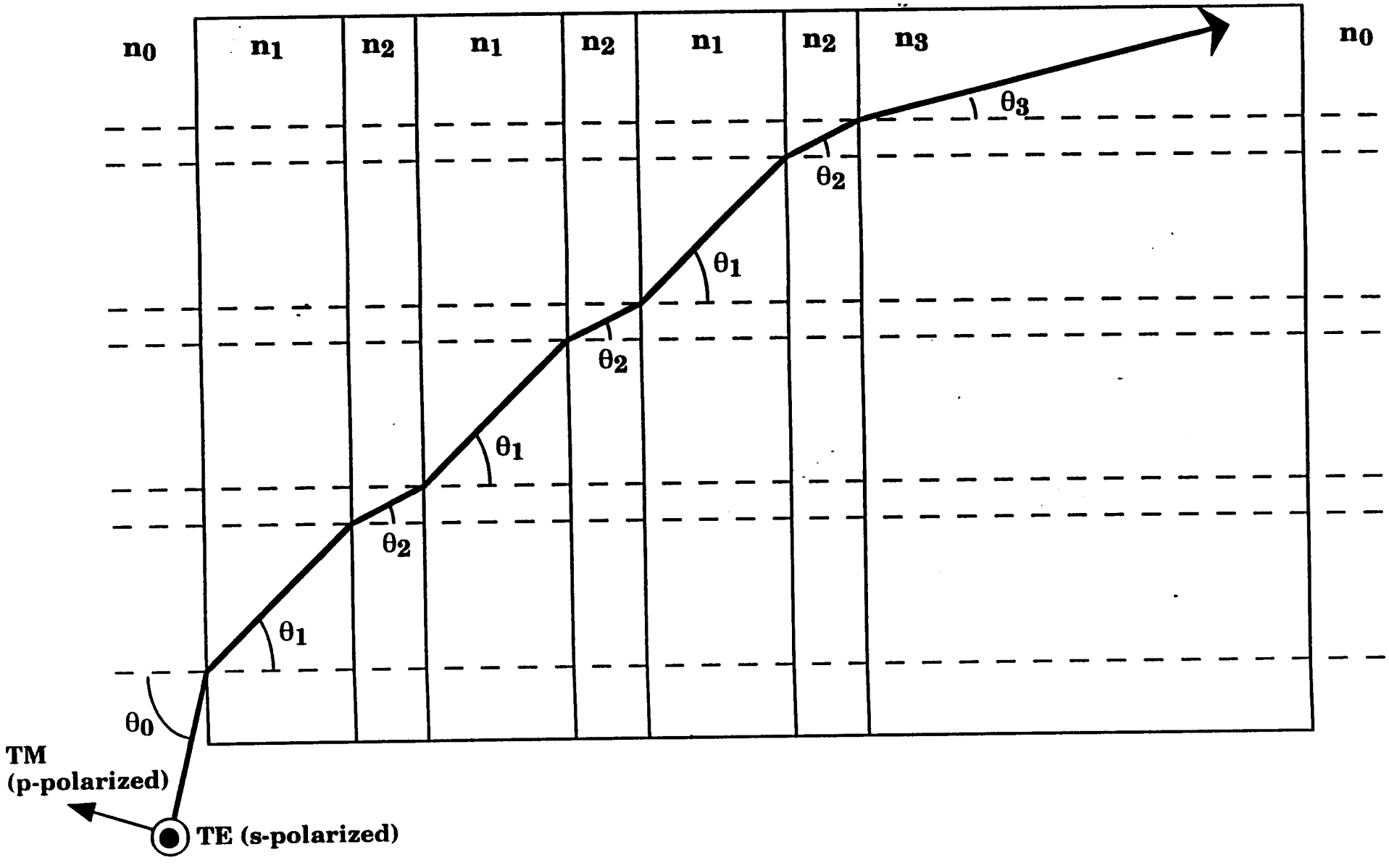
n0
n1
n2
n1
n2
n1
n2
n3
n0
θ3
θ2
θ1
θ2
θ1
θ2
θ1
θ0
TM
(p-polarized)
TE (s-polarized)

Fig. 9

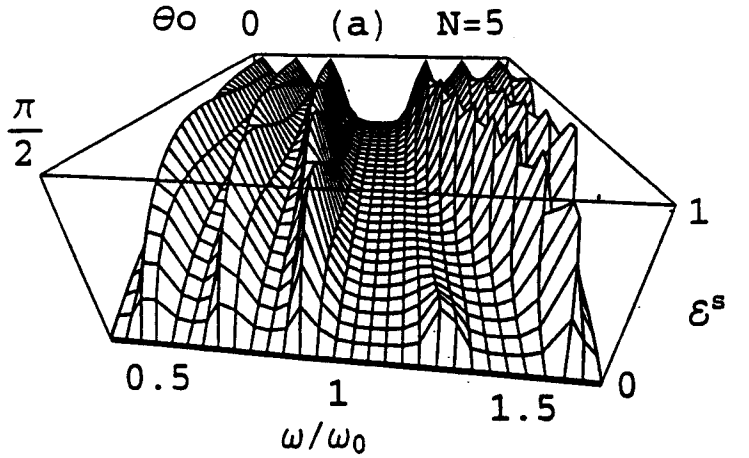
θo 0 (a) N=5
π/2
1
ε^s
0.5
1
1.5
0
ω/ω0

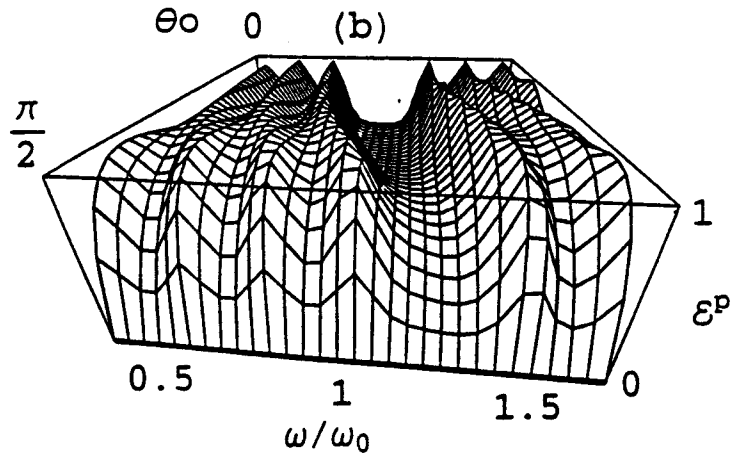
θo 0 (b)
π/2
1
ε^p
0.5
1
1.5
0
ω/ω0

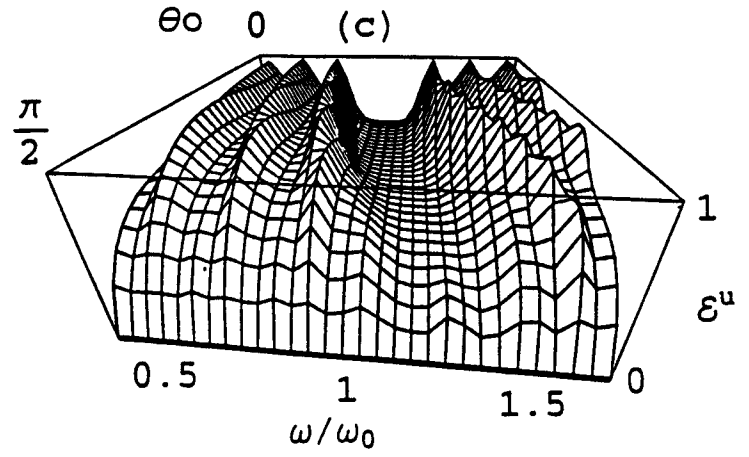
θo 0 (c)
π/2
1
ε^u
0.5
1
1.5
0
ω/ω0

Fig. 10